Direct observation of amide bond formation in a plasmonic nanocavity triggered by single nanoparticle collisions

Na Kong,^{†,‡} Jing Guo,[‡] Shuai Chang,[§] Jie Pan,[‡] Jianmei Wang,[†] Jianghao Zhou,^{‡,§} Jing Liu,[†] Hong Zhou,[†] Frederick M. Pfeffer,[†] Jingquan Liu,^ξ Colin J. Barrow,[†] Jin He,^{*,‡,†} and Wenrong Yang^{*,†}

†School of Life and Environmental Sciences, Deakin University, VIC 3216, Australia

[‡]Department of Physics, Florida International University, Miami, FL 33199, USA

[§] The State Key Laboratory of Refractories and Metallurgy, School of Chemistry and Chemical Engineering, School of Materials and Metallurgy, Wuhan University of Science and Technology, Wuhan, China

[§]College of Material Science and Engineering, Institute for Graphene Applied Technology Innovation, Qingdao University, Qingdao, Shandong, China

Biomolecular Science Institute, Florida International University, Miami, FL 33199, USA

Keywords: intermediates, amide bond formation, single nanoparticle collisions, single-entity EC-SERS.

ABSTRACT

The real-time observation of chemical bond formation at the single-molecule level is one of the great challenges in the fields of organic and biomolecular chemistry, and can provide information that is not accessible in ensemble-average measurements. Although remarkably sophisticated techniques for monitoring chemical reactions have been developed, the ability to detect the specific formation of a chemical bond in-situ at the molecules level has remained an elusive goal. Amide bonds are routinely formed from the aminolysis of N-hydroxysuccinimide (NHS) esters by primary amines, and the protocol is widely used for the synthesis, crosslinking and labeling of peptides and proteins. Herein, a plasmonic nanocavity was applied to study this single-molecule aminolysis reaction for amide bond formation, which was initiated by single nanoparticle collision events between suitably functionalised free-moving gold nanoparticles and a gold nanoelectrode in aqueous buffer. By means of simultaneous surface enhanced Raman spectroscopy (SERS) and single-entity electrochemistry (EC) measurements, we have probed the dynamic evolution of amide bond formation in the aminolysis reaction with 10 s of millisecond time resolution. Hence, we demonstrate single-entity EC-SERS is a valuable and sensitive technique by which chemical reactions can be studied at the level of a few molecules.

INTRUDUCTION

Direct observation of the bond making event at the single-molecule level, during the course of a chemical reaction, has been a longstanding goal for chemists. Probing dynamics of a chemical reaction with limited number of molecules can avoid the ensemble average, help reveal reaction pathways and identify transient intermediates, both of which are important for complete understanding of reaction mechanisms and the subsequent manipulation of reaction outcomes. Dynamic chemical reactivity investigations at the single-molecule level have been performed in the past decade, including the direct (and indirect) monitoring of conformational switching, chemical bonding and chemical reaction.¹⁻⁴ Indeed, individual reactant intermediates were observed during Cu(I)-catalyzed azide-alkyne cycloaddition (lifetime about 4.5 s) and bio-orthogonal cycloaddition processes (lifetime about 80 µs) by monitoring the ionic current flow through a well-designed protein nanopore. 5-6 Acceleration of a Diels-Alder reaction under external electric fields was observed using a scanning tunnelling microscopy break-junction approach. Non-contact atomic force microscopy was used to image a surface-catalysed cross-coupling and sequential cyclization cascade of 1,2bis(2-ethynyl phenyl)ethyne on Ag(100).7 However, these methods lack quantitative means of measuring chemical bond formation in real time. This challenge can be tackled by high temporal resolution micro-spectroscopic techniques, as they can provide valuable chemical fingerprint information during the chemical reaction process.3, 8-9 However, real-time observations of purrely single-molecule transient reaction with associated unambiguous chemical structure identification, applicable to chemical bond formation in solution, remains exceptionally challenging.^{3, 10-13}

To achieve single-molecule level detection of chemical reaction it is crucial to (i) obtain clear signals significantly above any background and to (ii) minimise instrument response time. ¹⁴ In the last decade, the surface enhanced Raman spectroscopy (SERS) has shown considerable promise for the detection of single-molecule behavious in the heterogenous chemical reactions in a plasmonic molecular junction. ¹⁵⁻¹⁶ The recent development of single-entity electrochemistry techniques also enablesfundamental individual nanoparticle (NP) collision events on a nanoelectrode (NE) to be investigated. ¹⁷⁻²² In addition to tracking of single NP dynamic motion and the sizing of individual NPs, the NP collision electrochemistry has been established as an effective strategy for (i) establishing intrinsic electrochemical parameters that

Commented [WY1]: Fred would suggest "only a few molcules"?

I would think if we could keep "single-molecule level"? Hou Jianguo's latest science paper used "single-molecule level plus others including Justin's works.

describe the mechanism of redox processes, and (ii) understanding electrochemical kinetics and interface charge transfer events, thus providing valuable additional information to that obtained using the conventional analysis. ²³⁻²⁶ The collision events of metallic NPs on metallic nanoelectrode result in the formation of dynamic plasmonic nanocavities in the nanoparticle-on-nanoelectrode (NPoNE) geometric configuration. 11 The use of a nanoelectrode not only reduces the nanoparticle collision frequency for the in situ SERS experiments toward to chemical reaction at the singlemolecule level, but also greatly decreases baseline noise, and this resolution offers an opportunity for monitoring chemical bond formation that approaches the singlemolecule level. Furthermore, it has been demonstrated that the well controlled electrochemical interface and confined space of a nanopore electrode provide a promising environment for evaluating chemical dynamics at the nanoscale. 27-31 Therefore, the simultaneous single-entity electrochemistry and SERS measurement system, designated as single-entity EC-SERS, can be a valuable tool to capture the detailed dynamic chemical changes during and after the formation of NPoNE geometry containing molecular junctions. In our recent works, 11, 32-33 the molecule level dynamic changes induced by metal-molecule interactions, intermolecular hydrogen bonds and host-guest interactions during and after the gold NP(GNP) 'hit-nstay' and 'hit-n-run' collision events on a chemically modified gold NE (GNE), have been probed with the single-entity EC-SERS techniques. These prior studies have led to an enhanced understanding of single NP dynamic motion near the molecule modified electrode surface and the associated molecular changes in the NPoNE structures. In this way, it has been possible to observe a variety of chemical bond formations in molecules transient reaction.

Amide bond formation is one of the most frequently used reactions in organic and biomolecular chemistry³⁴⁻³⁵ and represents one quarter of the reactions reported in small-molecule pharmaceutical patents.³⁶ Although recent advances in the mapping of amine-carboxylic acid coupling has enabled new amide coupling reactions³⁶, additional insight could guide the efficient design of even more efficient amide coupling reactions. In the present work, we provide a proof-of-concept demonstration that single-entity EC-SERS have been employed to study the coupling reaction between an NHS active ester and a primary amine in aqueous media at the single molecule level. First, formation of an amide bond was triggered by the individual GNP collision events at the GNE.

Importantly, the bond forming process was then monitored by EC-SERS with 10 s of millisecond time resolution. In addition, the stability of the formed molecular junction, and the electron transfer that occurs during, and after, amide bond formation were also examined by the enhanced electrochemical current and SERS, simultaneously in an nmwide nanogap. Due to the "click" reaction characteristics between NHS active ester groups and -NH₂ groups, the microscopic insights of aminolysis can directly indicate amide bond formation in this nm-scale gap region.

RESULTS AND DISCUSSIONS

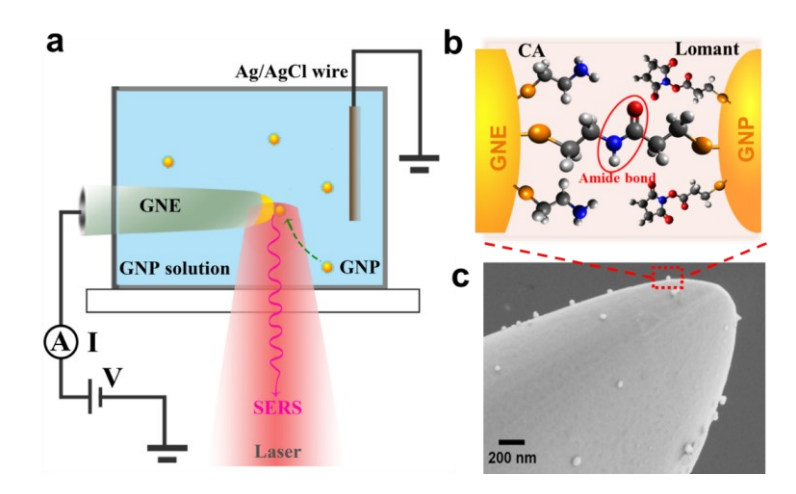


Fig. 1 | Single-nanoparticle collision measurements setup. a, Schematic of the EC-SERS measurement setup. **b**,The structure of the amide bond bridged GNE-molecule-GNP junction. **c**, SEM image of a GNE apex with GNPs that have landed on its surface.

As illustrated in Fig. 1a, a single-entity EC-SERS setup was used to monitor the dynamics of the chemical reaction at the GNE surface during GNP collision events. The SEM image in Fig. 1c shows a typical GNE with apex radius about 400 nm. Details of GNE fabrication and characterization are described in the methods and supporting information. To monitor amide bond formation, the GNE surface was functionalised with primary amine groups using cysteamine (CA) as the model amine substrate. This reagent possesses a flexible ethylene linker to the amine, such that conformational adjustments that are required during the reaction can be readily accommodated. The self-assembled monolayer (SAM) of CA molecules can also effectively suppress the direct electron transfer between redox probes and the GNE, which was confirmed by

cyclic voltammograms (CVs) of a GNE before and after the CA modification (Supplementary Fig. 1c). Based on the CV results and previously reported observations, 37 the density of CA on the electrode surface was estimated to be $\sim 10^{-9}$ mol/cm². The active ester group was introduced to the GNP surface by modifying the GNPs with Lomant's reagent (3,3'-Dithiodipropionic acid (bis *N*-Hydroxysuccinimide ester)). Due to the larger size of this moiety and the surface cuvature of the GNP, the number density of Lomant on the GNP surface should be smaller than that of CA on the GNE surface. The resulting Lomant-GNPs can be easily coupled to molecules containing primary amines through the formation of an amide bond. Detailed information for the modification and characterization of the Lomant-GNPs is given in the supporting information.

Active esters, such as the hydroxysuccinimidyl (NHS) esters featuring in Lomants reagent, have well-established use as acylation agents for the coupling of amino acids, peptides, proteins and other biomaterials, and in particular these esters are widely used for surface functionalization.^{20, 38} This versatility stems from their high stability in buffered aqueous solutions near physiological pH (6 to 9) and their rapid and selective reaction with free amine groups via aminolysis.³⁹ During a GNP collision event, when the Lomant-GNP arrives, the terminal amine groups of the modified GNE surface initiate amide bond formation; the reaction is triggered in the transiently formed NPoNE nanogap (illustrated in Fig. 1b). As shown in the SEM image (Fig. 1c), a number of Lomant-GNPs are discretely distributed on the surface of CA modified GNE apex, with a typical number density 11.4/µm² after the collision experiment. This observation is in line with our previous observations, 11,40 where only a few GNPs were found at the GNE apex. The SERS signals are mainly due to molecules inside the 'hotspot' of the NPoNE structure. Based on FDTD calculation, 32-33 the cross-section area of a NPoNE 'hotspot' was about 18 nm² and the estimated CA molecule number in a hotspot was around 100.41 Considering the low number of Lomant active esters in the same hotspot, only a handful of CA/Lomant pairs are expeted to undergo aminolysis in each NPoNE structure.

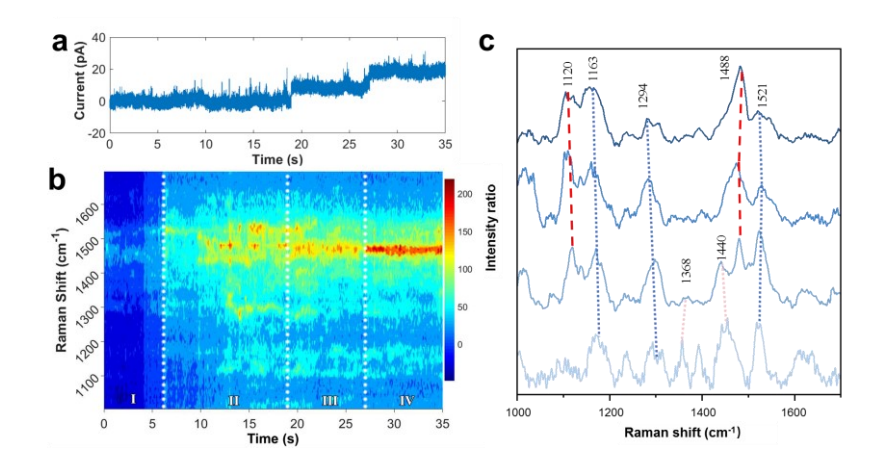


Fig.2 | Real-time monitoring of the single-nanoparticle collision events. a-b, Time-resolved electrochemical current trace (a) and the corresponding SERS trajectory (b) from a CA-GNE right after adding 20 pM Lomant-GNPs in 5 mM phosphate buffer containing 3 mM ferricyanide ions as the redox probes. c, The averaged SERS spectra after background correction from stages I to IV, which were further normalized to the highest peak.

Changes in electrochemical currents

Fig. 2a and b show the representative current-time (I-t) traces and time resolved SERS trajectory in heatmap format acquired simultaneously from a CA-GNE immediately after the addition of Lomant-GNPs. We first analysed the current changes induced by the GNP collision events. The GNE was applied a bias at 600 mV vs. Ag/AgCl quasi reference electrode, which is needed to generate EC current from the oxidation of Fe(CN)₆⁴ ions in solution. Before adding Lomant-GNPs to the solution, no detectable current change could be observed (Supplementary Fig. 5a). After the Lomant-GNPs were added, upward current changes were frequently and clearly evident, induced by the increased oxidation current from the Fe(CN)₆⁴ ions. The newly landed GNP could restore electron transfer between electrode and solution redox species supressed by the SAM. 42-43 Three types of current changes were observed: (i) single spikes, (ii) cluster spikes and (iii) staircase signals (Fig. 3). The experimental timeframe was approximatelyabout 20 minutes. Notably, the individual current spikes were the dominant changes apparent in the I-t trace, and changes assignable to cluster spikes were less evident. The current steps were most distinguishable for a short time immediately following the addition of the Lomant-GNPs to the solution. The collision event rate generally varies over time. In average, we observed a mean rate of 0.73 events/s. The theoretical collision rate based on the diffusion model was calculated to be 0.39 events/s. The higher experimental value can be explained by the electrophoretic motion of the GNP due to the applied electric field. Also, one GNP collision event may generate multiple events due to Brownian motion. 18, 24, 44

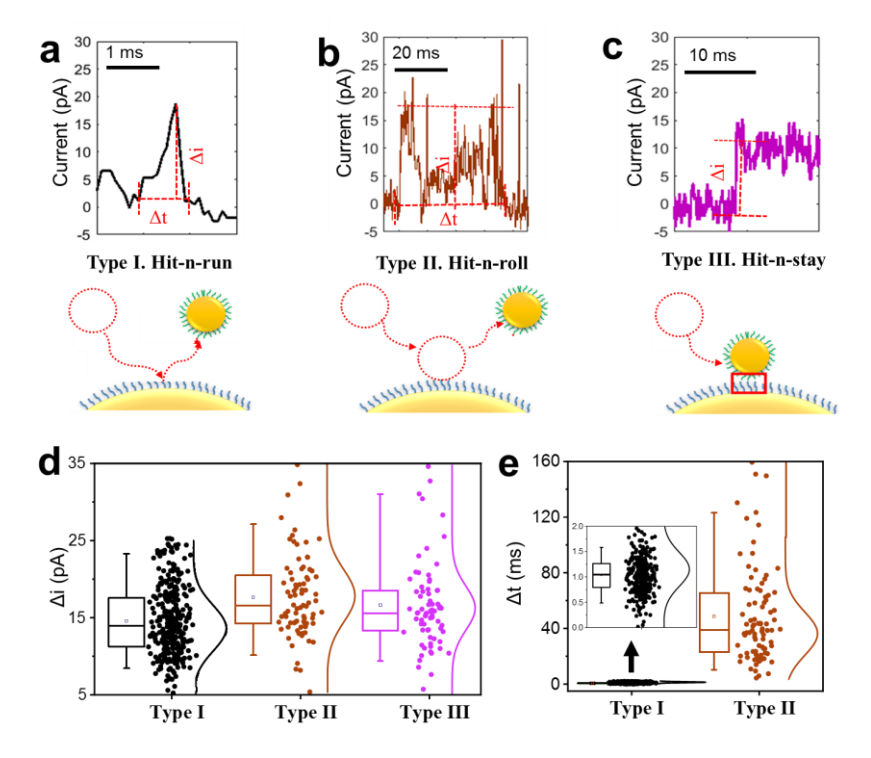


Fig. 3 | Three types of current responses identified in the typical I-t traces. a, single current spike (black color), b, clusters of current spikes (brown color) and c, step current changes (purple color). Middle raw: the proposed scheme of corresponding collision events: I) hit-n-run, II) hit-n-roll, III) hit-n-stay. d, The box charts show the distribution of peak current height (Δi) and e, residence time (Δt) corresponding to three types respectively. (The middle line and square in the box chart demote the median and mean value of associate box).

The EC current changes can be used to reveal the motion of the GNP during and after collision.^{17, 45} Previous nano-impact studies have demonstrated that the motion of GNP in collision events gives rise to two distinct current changes: a cumulative cascade of current (or 'staircase') steps and a series of transiently decaying current jumps (spikes). A current staircase is expected for a 'hit-n-stay' event which correlates with the long-

term attachment of a GNP, while the current spikes are attributed to 'hit-n-run' events where the GNP has a short residence time at the GNE surface. Here, three types of current changes were observed as illustrated in Fig.3 (shown along with the distributions of peak current (Δi) and residence time (Δt)). The dominant current spike (Fig. 3a), 67.3% of all the events, was interpreted to be the result of 'hit-n-run' (Type I) collision events where interfacial interactions are weak. The mean amplitude of these spikes is about 14.5 ± 0.5 pA with a duration time of 1.1 ± 0.1 ms.

In Fig. 3b a cluster of current spikes with apparent longer duration are shown, with fluctuations in peak shape, height and duration. Importantly, however, the current returns to its original level. These clustered current spikes could be explained by 'hit-and-roll' behaviour. It is also possible that a single GNP can experience multiple-collision events (Type II). $^{24,\,48}$ When a Lomant-GNP collides and lands on the GNE surface, chemical interactions impede the motion of the GNP but not enough to instantly stop the motion of GNP. Therefore, the Lomant-GNP fluctuates on the GNE surface, resulting in rapid changes in the measured current and in turn to the observed clustered spikes. Statistically, there are 17.9% of type II events. The mean current spike magnitude is 17.4 \pm 0.8 pA and the residence time is 48.7 \pm 6.0 ms, both are significantly larger than the corresponding values of the current spikes in 'hit-n-run' events.

The last 'step' type current pattern (Fig. 3c) represents a 'hit-n-stay' collision event (Type III), which represents 14.8% of the total number of events. During the 'hit-n-stay' collision process, Lomant-GNPs stay on the electrode surface after the collision and a long-term current increase is induced. The mean current magnitude is 16.5 ± 0.6 pA, which is close to the mean value of the current changes in 'hit-n-roll' events. The values of Δi are closely dependent on the strength of the electronic coupling of the formed molecular links, which is the NHS ester/amine interface. The residence time also reflects the binding strength of the weak link. The increased Δi and Δt in types II and III events suggest that the interaction between the NHS active ester and the amine groups is stronger than type I and is indicative of covalent bond formation.

Dynamic changes in time-resolved SERS trajectory

To further understand the dynamic interaction, and reaction, between the NHS ester and the amine groups during and after the collision process, we investigated the time-

resolved SERS spectra recorded at the same time. 11, 49-50 No detectable Raman signal could be observed before adding Lomant-GNPs (Supplementary Fig. 5b). The SERS time trajectory in Fig. 2b reveals the spectral changes within the hotspot of NPoNE cavities immediately after adding the Lomant-GNPs. Four main stages in Fig. 2b were identified based on both the EC current and spectral changes. With the landing of GNPs on the GNE through collision events, the intensity of molecule vibration peaks along with the backound gradually increases. The evolution of the background intensity during four stages is shown in Supplementary Fig. 3d. In addition to intensity increase, there is a small redshift about 1.8 nm in wavelength (34 cm⁻¹ in Raman shift) of the background maximum from stages I to IV. This is attributed to the changes of nanocavity properties induced by the landing of a few GNPs on the GNE apex. 51-53 Following the previously reported method, 54 we also corrected the SERS spectra ((raw -backgound)/background) to avoid background influence (see Supplemetray Fig. 3). The averaged SERS spectrum from these four stages after background correction and normalization are shown in Fig. 2c. First, in stage I (from 0 to ~6 s), following the addition of Lomant-GNPs in solution, weak and discrete SERS blinking signals were occasionally observed. Combined with the type I current changes that appeared at the same time in the I-t trace shown in Fig. 2a, most Lomant-GNPs likely rebounded quickly from the GNE surface after the collision with the CA-GNE. Due to the short residence time of the Lomant-GNPs, the transient GNP-Lomant-CA-GNE junction gives rise to the blinking and weak SERS signals. Next, in stage II (from ~6 to ~19 s), a significantly increased number of SERS blinking signals were observed along with more clustered current spikes, corresponding to an increased number of 'hit-n-roll' events of the GNPs. It is possible that GNPs may 'dance' near the GNE surface and the SERS signals are highly dynamic at this stage but gradually increased in their overall intensity. In particular, a new peak at 1480 cm⁻¹ appeared near 11 s, which was also identified in the averaged spectra of stage II (Fig.2c). Stage III begins with a clear current step in the I-t trace near 19 s due to a 'hit-n-stay' event. In concert with this event, the SERS signals became more stable and the new peak at 1480 cm⁻¹ became prominent. Finally, at the beginning of stage IV, a second current step appeared at 27.3 s with a similar step height to the first current step that occurred at the beginning of stage III. When the second 'hit-n-stay' signal was observed, the 1480 cm⁻¹ peak again increased its intensity sharply and slightly blue-shifted to 1488 cm⁻¹. Enhancements in overall Raman signal intensity and stability were evident. After this event, the spertra

remained relatively stable for the rest of the measurement. Furthremore, the intensity time traces near 1500 cm⁻¹ and 1120 cm⁻¹ over the whole 20 minutes measurement time were followed (Supplementary Fig. 4a). The overall intensity of SERS spectroscopy increased rapidly in the first minute but was relatively stable afterwards. Therefore, the number of strongly attached GNPs on the GNE apex are likely very limited. The peak near 1480 cm⁻¹ may also be affected by the possible carbon bands near 1350 and 1580 cm⁻¹, which are from the decomposition of probe molecule and carbon-related residues (contamination).⁵⁵⁻⁵⁶ However, the long-term stability of the peak near 1480 cm⁻¹ (as shown in Supplemtary Fig. 4a and b) over the whole measurement time suggests the carbon effect is negnigible, especially at the first a few minutes.

To better understand the spectral changes that occurred during the collisions of the Lomant-GNPs with the CA-GNE, a series of control experiments were conducted using (i) CA-GNE and unfunctionalised GNPs, and (ii) bare GNE and Lomant-GNPs. The corresponding Raman spectra obtained from CA powder, and GNP-CA-GNE and GNP-Lomant-GNE structures, are shown in supplementary Fig. 6, with the peak assignment summarized in Table S1. In the first control experiment, the dynamic changes in EC current and SERS spectra reveal the fast formation of stable GNP-CA-GNE molecular junctions, induced by the amine-Au interaction during GNP collision events.⁵⁷ The SERS spectra of CA in the NPoNE streutrue were very different from those shown in Fig. 2b. In the second control experiment, a broad bump between 1400 and 1550 cm⁻¹ gradually appeared in the SERS trajectory, which was attributed to the formation of GNP-Lomant-GNE nanostructure through non-covalent interactions. The dynamic spectral changes observed in both control experiments were very different from the results in Fig. 2b. Therefore, the unique dynamic spectral changes observed in Fig. 2b are a direct result of interaction between CA and the NHS active ester of the Lomant functionalised GNP.

In another control experiment, 3-Mercaptopropionic acid (3-MPA) SAM was formed on the GNE apex to render a GNE surface with –COOH terminal groups. After adding Lomant-GNPs to the solution, both the I-t and time-resolved SERS spectra were acquired to record the Lomant-GNPs collision events at the 3-MPA-GNE surface (Supplementary Fig. 7). In the I-t trace, only individual current spikes (like type I spike) and occasional clusters of spikes were observed, implying the interaction between 3-

MPA and Lomant was relatively weak. In the SERS spectra, a broad band between 1400 and 1550 cm⁻¹ was observed, which was attributed to the Lomant active ester.

DFT calculations

Density functional theory (DFT) simulations were performed to further interpret the spectral changes observed in the time-resolved SERS trajectories during the GNP collision events. According to a number of previous kinetic and mechanistic studies in which the aminolysis (an addition/elimination reaction) of esters, including NHS esters in aqueous solution, a tetrahedral intermediate is initially formed after nucleophilic addition of the amine to the C=O bond of the active ester. S8-60 As shown in Fig. 4a, when the Lomant-GNPs (containing NHS active ester groups) make physical contact with the electrode surface at neutral pH, the primary amine groups react with the ester and the product of this initial nucleophilic attack, a tetrahedral intermediate (zwitterion 1 in Fig. 4a) can be formed. With loss of a proton and the intramolecular elimination of the –OSu group from 1, the amide product is formed.

The molecular structures and Raman spectra of reactant Lomant and the amide product are shown in Fig. 4b and c, respetively. The vibration-mode assignments of reactants and product are outlined in Tables S1 and S2. 50, 61 The Raman spectra of reactant CA and Lomant reagent and the SERS spectra of GNP-CA-GNE and GNP-Lomant-GNE are shown in supplementary Fig. 6. The contributions of CA are generally much weaker and will not be discussed here. In the calculated spectrum of Lomant, the two peaks in the 1400-1500 cm⁻¹ range are higher than others and they are the ν (O-N-C) from the hydroxysuccinimide (–OSu) group and the CH₂ vibrations from both the –OSu group and the backbone of Lomant. In the calculated spectrum of the amide product, the major peak near 1463 cm⁻¹ is the amide II vibrations. Several peaks located near 1100-1300 cm⁻¹ are assigned to the C-N vibrations of amide III.

We also calculated the Raman spectra of intermediate 1. Because its structure was unstable in the DFT calculation, we calculated the alternative structure 1' (Fig. 4b), which is formed by transferring one proton from the -NH₂⁺ to -O⁻. We also calculated another alternative structure 1'-F by introducing a fluoride atom near the oxygen atom. The F atom serves as an electron withdrawing group (EWG) to mimic the negatively charged oxygen in 1 for calculation purposes. The calculated Raman spectra are shown in Fig. 4d. For both structures, the major peaks are both close to 1440 cm⁻¹, which are

from the the v(O-N-C) vibration of the -OSu group. The amide II vibration of the formed C-N bond is supressed by the -OSu group and cannot be distinguished. The blue-shift of the major peak in the 1400-1550 cm⁻¹ spectral range from the Lomant and aminolysis intermediate to the final product is attributed to the departure of the -OSu group after the amide bond formation. A similar phenomena has been observed during simple carbodiimide mediated peptide coupling in aqueous solution. 62

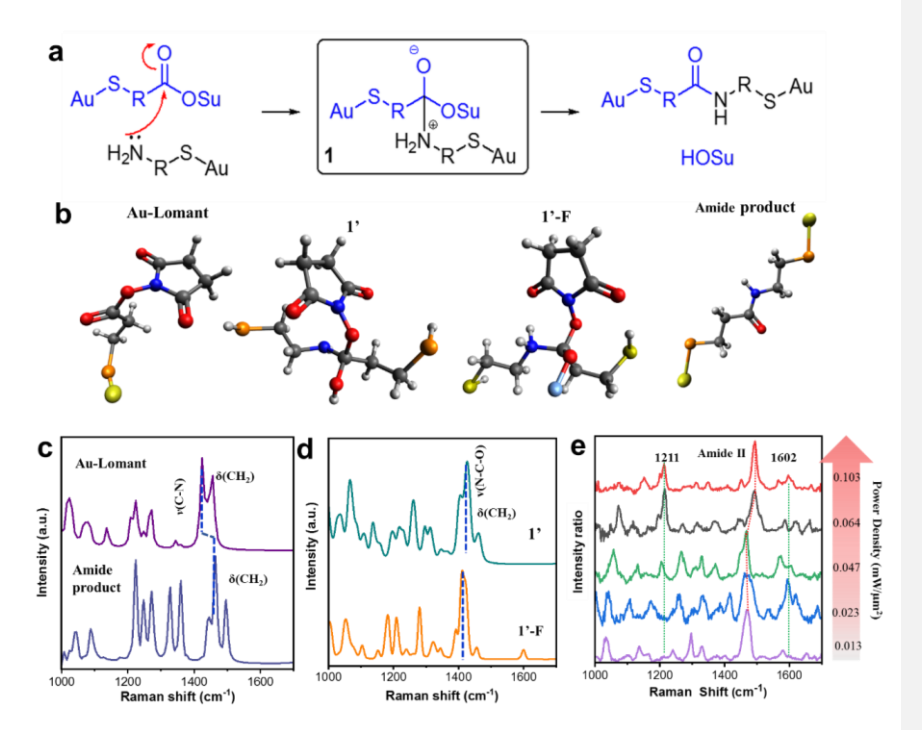


Fig. 4 | The DFT simulation results and proposed aminolysis reaction route. a, Mechanistic illustration of the aminolysis reaction between the Lomant-GNP and CA-NE. b, Structure of Au-Lomant, intermediate 1', intermediate 1'-F and the amide product. c-d, The calculated Raman spectra of Au-Lomant and Au-Amide product-Au (c) and intermediate 1', intermediate 1'-F (d). e, The SERS spectra (after background correction) of amide product with various power density (mW/ μ m²), which was further normalized to the Amide II peak.

Based on the DFT calculations, we postulated that the appearance and blue-shift of the pronounced new peak near or higher than 1480 cm⁻¹ is the spectral evidence of aminolysis reaction between NHS active ester and amine in the nanocavity during the 'hit-n-roll' and 'hit-n-stay' events. In the experiment, there was often a broad bump in the 1400-1550 cm⁻¹ range, which can be attributed to the flexible orientations of –OSu

groups and the possible intermediates in the nanocavity. When new amide bonds are formed a new peak appears near 1480 cm⁻¹ that is sharp and clearly resolved above the 'bump' in the SERS spectrum. In contrast, the peak near 1440 cm⁻¹ becomes indistingushable due to the cleavage of -OSu groups. The correlated current increase with the peak intensity of 1480 cm⁻¹ also supports the formation of amide bonds, which bridge the junction and improve the electron transport process. After the appearance of the prominent peak near 1480 cm⁻¹, both the current and Raman spectra become stable with minimal fluctuations. The increased stability of the nanocavities is likely due to the newly formed covalent bonds. The aminolysis reaction in the hotspot of the NPoNE geometry can also be accelerated by light. As shown in Fig. 4e, with the increase of incident light intensity, the most noticible change is that the v(C-N) peak of amide II band becomes sharper and is blue-shifted from the broader peak near 1473 cm⁻¹ to 1501 cm⁻¹. The shaprend amide II peak at the higher laser intensity also suggest carbon comtamination induced by probe molecule degradation is not likely in our measurements.⁵⁶ The peak near 1211 cm⁻¹ is attibued to the C-N vibration (amide III) of the backbone of the formed amide product, which is not obvious at the lower light intensity. The peak near 1602 cm⁻¹ is likely due to the C=O of Amide I.⁴¹

Amide bond formation induced dynamic spectral changes in collision events

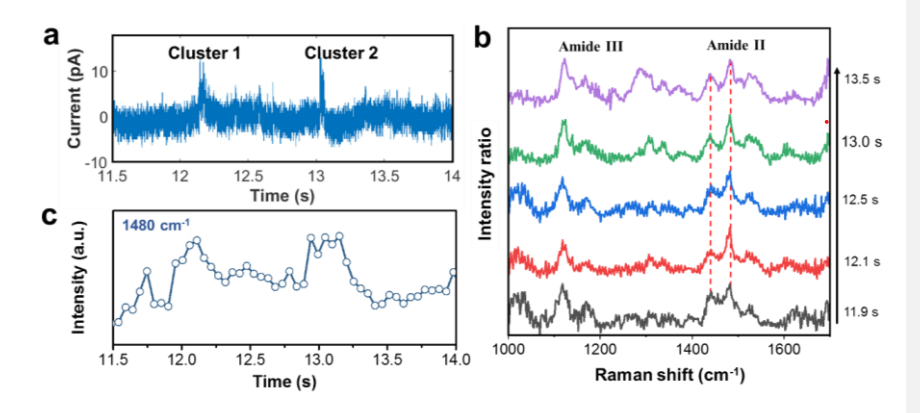


Fig. 5 | Transient SERS changes induced by 'hit-n-roll' collision events of Lomant-GNPs. a, Simultaneously recorded electrochemical current trace (blue) induced by 'hit-n-roll' collision events of Lomant-GNPs. **b**, Selective SERS spectra (after background correction and normalization) in the spectral range of 1000 to 1700 cm⁻¹ from 11.9 to 13.5 s. **c**, The corresponding SERS intensity-time trace at band 1480 cm⁻¹.

After investigated the overall changes of the SERS and EC current signals triggered by the collision events of Lomant-GNPs on CA-GNE, we further examined the detailed changes induced by 'hit-n-roll' and 'hit-n-stay' events in the I-t trace and SERS trajectory. From the long I-t trace shown in Fig. 2a, a small section has been expanded (Fig. 5a) to show two current spikes, appearing at 12.2 and 13.0 s. They are type II spikes (Supplementary Fig. 8a), which are attributed to the 'hit-n-roll' collision events of Lomant-GNPs. The corresponding SERS signal changes in heatmap format were also recorded (Supplementary Fig. 8b) and five SERS transient spectra after background correction and normalization are shown in Fig. 5b. The appearance of the sharp peak near 1480 cm⁻¹, attributed to v(C-N) of amide II, indicates the existence of amide-bond products due to aminolysis. The neighboring peak near 1440 cm⁻¹, assigned to the v(O-N-C) vibration, suggests a number of Lomant molecules coexisit in the hotspot. The peak near 1525 cm⁻¹ was assigned to the bending mode of CH₂ linker. Because the v(C-N) mode at 1480 cm⁻¹ can only come from the amide product, it can be used to reveal the aminolysis reactions in the hotspot. As shown in the intensity-time trajectory of Fig. 5c, the intensity of the peak at 1480 cm⁻¹ increased with the arrival of the Lomant-GNP and decreased when it left. The duration of the two current spikes are 49 and 41 ms respectively, while the 1480 cm⁻¹ peak remained at an elevated intensity for a much longer time than the current signals. The time mismatch suggests that the Lomant-GNP along with the formed amide-bonds stays longer on the GNE surface during the two 'hit-n-roll' events, while effective electron transfer across the junction only happens for a much shorter time.

In contrast to the transient changes noted for a 'hit-n-roll' event, the 'hit-n-stay' collision events produce persistent changes. Two examples are shown in the SERS heatmap in Fig. 2b at about 19 and 27 s. After the event at 19 s, the amid II peak near 1480 cm⁻¹ stands out and becomes much higher than others. Meanwhile, the 1440 cm⁻¹ peak cannot be differentiated. Another 'hit-n-stay' event at 27 s, introduces another sudden jump in the intensity of the amide II peak near 1488 cm⁻¹, which remains stable afterwards. Obviously, these two 'hit-n-stay' events form stable hotsopt and trigger more aminolysis reactions, which greatly increase the number of amide bonds formed in the hotspot.

Another case of a 'hit-n-stay' event is shown in Fig. 6 (also see Supplementary Fig. 9). The time-resolved spectral change is displayed in Fig. 6a. Before 36.3 s, the features in

the spectra were similar with those of the spectra in stage II of Fig. 2b, suggesting the number of formed amide bonds is low. With the stable landing of a new Lomant-GNP at 36.3 s, signalled by a stepwise current jump, the v(C-N) peak of the amide band II suddently blue-shifted about 20 wavenumbers and its intensity also increased noticably. This clear transition suggests that most of the molecules in the hotspot undergo aminolysis reaction, triggered by the GNP collision event. Along with the spectral change of v(C-N) mode of amide II, the peaks at 1130 and 1540 cm⁻¹ also increase obviously after the 'hit-n-stay' event. Based on the DFT calculations, they are likely the stretching mode of C-N (amide III) and the bending mode of CH₂, respectively, of the final amide product.

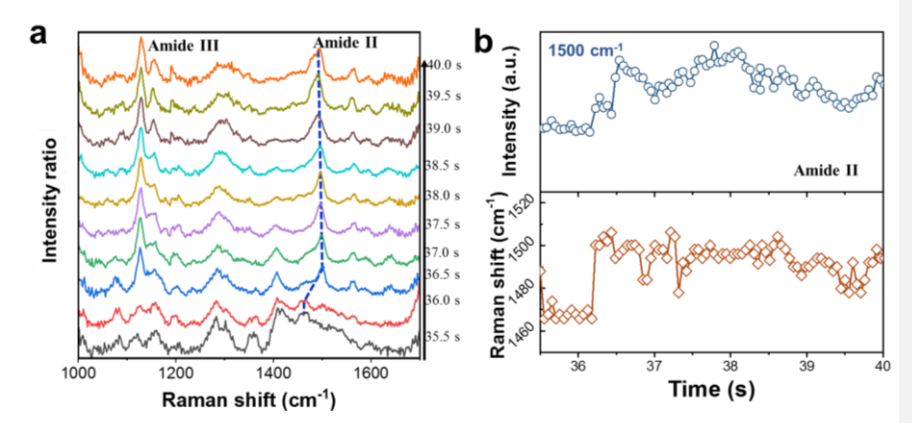


Fig. 6 | Time-resolved SERS changes induced by a 'hit-n-stay' collision event of Lomant-GNPs. a, Progressive SERS spectra after background correction and normalization. b, The time traces of intensity (top panel) and Raman shift (bottom panel) of the v(C-N) mode of amide II band.

CONCLUSIONS

In this work, we probed the intermolecular reaction between primary amine groups on the surfaces of a modified GNE with active NHS esters appended to free-moving GNPs in a buffer solution through simultaneous time-resolved SERS and EC chronoamperometry measurements. The individual GNP collision events can be tracked based on EC current changes and the triggered aminolysis reactions have been successfully monitored based on the spectral changes of the amide vibration modes in the SERS measurements. The reaction 'yield' is low in the transient 'hit-n-run' and 'hit-n-roll' events but much higher after the 'hit-n-stay' events. Observing the intricate

chemical transformation that occurs during chemical reaction is of great importance for exploring reaction mechanisms and may lead to dramatic improvements in industrially relevant processes. Traditional reaction identification techniques are somewhat limited in terms of sensitivity, selectivity, time-resolution and a focussed analysis environment, 4 while the single-entity EC-SERS technique satisfies the required criteria for most chemical reactions. It is likely that this single-nanoparticle approach to observe the dynamic formation of covalent bond formation can also be applied to other important chemical reactions.

METHODS

Materials. GNPs with a diameter of 40 nm were purchased from Ted Pella, Inc. The GNPs were functionalized by Lomant regents to form NHS ester terminated surface by self-assembly method. The GNEs were electrochemically etched to form sharp apexes with relatively smooth electrode surface, as described in the previous report. The etched GNE was partially insulated with melted high density polyethylene (HDPE) to expose the apex. The prepared GNEs were electrochemical cleaned in 0.5 M H₂SO₄ electrolyte by repeated potential scans between 0 and 0.9 V at a scan rate 50 mV/s. After electrochemical cleaning, the GNEs were immersed in 5 mM molecule solution (in ethanol) for 4 hours to form a SAM over exposed surface of GNE apex.

EC-SERS measurements: Detailed EC-SERS spectroscopy measurement setups were reported previously and only briefly described below.¹¹ The GNE was placed in a liquid cell on the sample stage of a Nikon Inverted Microscope (Eclipse, Ti-U). A 632.8 nm HeNe laser was focused on the GNE with a beam radius about 3 μm and typical powder density about 0.047 mW/μm². Raman signal passed through a spectrograph (Acton SP 2356, Princeton Instrument) was recorded by a CCD camera (PIXIS 100B_eXcelon, Princeton Instrument). The spectrum resolution was about 2 cm⁻¹. The typical time resolution used for the time-resolved SERS trajectory was 51.9 ms. An Axon 200B patch-clamp amplifier (Molecular Devices Inc., CA) in voltage-clamp mode was used to supply the electrode potential and amplify the current. A 10 kHz Bessel low-pass filter was typically used for the EC current measurements. The EC data was recorded at 50 kHz by an Axon Digidata 1440A (Molecular Devices Inc., CA), which was synchronized with the CCD camera. The obtained data were analyzed by

custom Labview (National Instruments) and Matlab (MathWorks Inc.) programs. The current spikes were detected by a threshold event detection method.⁶⁶⁻⁶⁸

ASSOCIATED CONTENT

Supporting Information

The Supporting Information is available free of charge on the ACS Publications website at DOI:

detailed materials and methods, preparation, characterization of GNE and Lomant-GNPs, control experiments of unfuctionalized GNPs with CA-GNE and Lomant-GNPs on bare GNEs, the assignment of SERS peaks of the corresponding control experiments, description of Raman spectra simulations by Density Functional theory (PDF).

AUTHOR INFORMATION

Corresponding Authors

*E-mail: wenrong.yang@deakin.edu.au.

*E-mail: jinhe@fiu.edu.

ORCID:

Na Kong: 0000-0002-5010-8744 Shuai Chang: 0000-0001-7405-5555

Frederick M. Pfeffer: 0000-0002-5441-6437 Colin J. Barrow: 0000-0002-2153-7267

Jin He: 0000-0002-2633-9809

Wenrong Yang: 0000-0001-8815-1951

Notes

The authors declare no competing financial interest.

ACKNOWLEDGEMENTS

The authors acknowledge the Australian Research Council for primary support of this work under Grant No. DP130101714 (W.Y) and Victoria International Research Scholarship (N.K.). This work was partially supported by NSF CBET-1454544 and CHE-2003785. J. G was supported by the Engineering Research Centers Program of the National Science Foundation under NSF Cooperative Agreement No. EEC-1647837.

18

REFERENCES

- (1). Aragonès, A. C.; Haworth, N. L.; Darwish, N.; Ciampi, S.; Bloomfield, N. J.; Wallace, G. G.; Diez-Perez, I.; Coote, M. L. *Nature* **2016**, *531*, 88-91.
- (2). Kim, K. H.; Kim, J. G.; Nozawa, S.; Sato, T.; Oang, K. Y.; Kim, T. W.; Ki, H.; Jo, J.; Park, S.; Song, C.; Sato, T.; Ogawa, K.; Togashi, T.; Tono, K.; Yabashi, M.; Ishikawa, T.; Kim, J.; Ryoo, R.; Kim, J.; Ihee, H.; Adachi, S.-i. *Nature* **2015**, *518*, 385-389.
- (3). Zhou, C.; Li, X.; Gong, Z.; Jia, C.; Lin, Y.; Gu, C.; He, G.; Zhong, Y.; Yang, J.; Guo, X. *Nat. Commun.* **2018**, *9*, 807.
- (4). Guan, J. X.; Jia, C. C.; Li, Y. W.; Liu, Z. T.; Wang, J. Y.; Yang, Z. Y.; Gu, C.
- H.; Su, D. K.; Houk, K. N.; Zhang, D. Q.; Guo, X. F. Sci. Adv. 2018, 4, eaar2177.
- (5). Qing, Y.; Pulcu, G. S.; Bell, N. A.; Bayley, H. *Angew. Chem., Int. Ed.* **2018**, *130*, 1232-1235.
- (6). Luchian, T.; Shin, S. H.; Bayley, H. Angew. Chem., Int. Ed. 2003, 42, 3766-3771.
- (7). Riss, A.; Paz, A. P.; Wickenburg, S.; Tsai, H. Z.; De Oteyza, D. G.; Bradley, A. J.; Ugeda, M. M.; Gorman, P.; Jung, H. S.; Crommie, M. F.; Rubio, A.; Fischer, F. R. *Nat. Chem.* **2016**, *8*, 678-683.
- (8). Xiang, L.; Tao, N. J. Nature 2016, 531, 38.
- (9). Cao, Y. W. C.; Jin, R. C.; Mirkin, C. A. Science 2002, 297, 1536-1540.
- (10). Zewail, A. H. J. Phys. Chem. A 2000, 104, 5660-5694.
- (11). Guo, J.; Pan, J.; Chang, S.; Wang, X.; Kong, N.; Yang, W.; He, J. Small 2018, 14, e1704164.
- (12). Kuramochi, H.; Takeuchi, S.; Iwamura, M.; Nozaki, K.; Tahara, T. *J. Am. Chem. Soc.* **2019**, *141*, 19296-19303.
- (13). Heo, J.; Ahn, H.; Won, J.; Son, J. G.; Shon, H. K.; Lee, T. G.; Han, S. W.; Baik, M. H. *Science* **2020**, *370*, 214-219.
- (14). Wu, Y.; Bennett, D.; Tilley, R. D.; Gooding, J. J. Adv. Mater. **2020**, *32*, 1904339.
- (15). Choi, H. K.; Park, W. H.; Park, C. G.; Shin, H. H.; Lee, K. S.; Kim, Z. H. *J. Am. Chem. Soc.* **2016**, *138*, 4673-84.
- (16). Choi, H.-K.; Lee, K. S.; Shin, H.-H.; Koo, J.-J.; Yeon, G. J.; Kim, Z. H. Acc. Chem. Res. **2019**, *52*, 3008-3017.
- (17). Xiao, X.; Bard, A. J. J. Am. Chem. Soc. 2007, 129, 9610-9612.
- (18). Kang, M.; Perry, D.; Kim, Y.-R.; Colburn, A. W.; Lazenby, R. A.; Unwin, P. R. J. Am. Chem. Soc. **2015**, 137, 10902-5.
- (19). Jung, A. R.; Lee, S.; Joo, J. W.; Shin, C.; Bae, H.; Moon, S. G.; Kwon, S. J. J. Am. Chem. Soc. **2015**, 137, 1762-1765.
- (20). Li, D.; Kong, N.; Liu, J. Q.; Wang, H. B.; Barrow, C. J.; Zhang, S. S.; Yang, W. R. *Chem. Commun.* **2015**, *51*, 16349-16352.
- (21). Wang, Y.; Shan, X.; Tao, N. Faraday Discuss. 2016, 193, 9-39.
- (22). Baker, L. A. J. Am. Chem. Soc. 2018, 140, 15549-15559.
- (23). Ma, W.; Ma, H.; Chen, J. F.; Peng, Y. Y.; Yang, Z. Y.; Wang, H. F.; Ying, Y. L.; Tian, H.; Long, Y. T. *Chem. Sci.* **2017**, *8*, 1854.
- (24). Oja, S. M.; Robinson, D. A.; Vitti, N. J.; Edwards, M. A.; Liu, Y.; White, H. S.; Zhang, B. *J. Am. Chem. Soc.* **2017**, *139*, 708-718.
- (25). Peng, Y. Y.; Qian, R. C.; Hafez, M. E.; Long, Y. T. ChemElectroChem 2017, 4.
- (26). Wei, X.; Zou, G.; Hou, H.; Ji, X. Small **2019**, 15.

- (27). Ying, Y. L.; Long, Y. T. Sci. China. Chem. 2017, 1-4.
- (28). Yi-Lun; Ying; Yong-Xu; Hu; Rui; Gao; Ru-Jia; Yu; Zhen; Gu J. Am. Chem. Soc. 2018.
- (29). Gao, R.; Lin, Y.; Ying, Y.-L.; Hu, Y.-X.; Xu, S.-W.; Ruan, L.-Q.; Yu, R.-J.; Li, Y.-J.; Li, H.-W.; Cui, L.-F.; Long, Y.-T. *Nat. Protoc.* **2019**, *14*, 2015-2035.
- (30). Yu, R. J.; Xu, S. W.; Paul, S.; Ying, Y. L.; Long, Y. ACS Sens. 2020, 6.
- (31). Yu, R.-J.; Xu, S.-W.; Paul, S.; Ying, Y.-L.; Cui, L.-F.; Daiguji, H.; Hsu, W.-L.; Long, Y.-T. *ACS Sensors* **2021**, *6*, 335-339.
- (32). Liu, Z.; Liu, J. Q.; Mateti, S.; Zhang, C. M.; Zhang, Y. X.; Chen, L. F.; Wang,
- J. M.; Wang, H. B.; Doeven, E. H.; Francis, P. S.; Barrow, C. J.; Du, A. J.; Chen, Y.; Yang, W. R. *Acs Nano* **2019**, *13*, 1394-1402.
- (33). Ai, Q.; Zhou, J.; Guo, J.; Pandey, P.; Liu, S.; Fu, Q.; Liu, Y.; Deng, C.; Chang, S.; Liang, F.; He, J. *Nanoscale* **2020**, *12*, 17103-17112.
- (34). Montalbetti, C. A.; Falque, V. Tetrahedron 2005, 61, 10827-10852.
- (35). Brown, D. G.; Bostrom, J. J. Med. Chem. 2015, 59, 4443-4458.
- (36). Mahjour, B.; Shen, Y.; Liu, W.; Cernak, T. Nature 2020, 580, 71-75.
- (37). Wirde, M.; Gelius, U.; Nyholm, L. Langmuir 1999, 15, 6370-6378.
- (38). Neouze, M.-A.; Schubert, U. Monatsh. Chem. 2008, 139, 183-195.
- (39). Yellin, N.; Levin, I. W. Biochemistry 1977, 16, 642-647.
- (40). Ma, T.; Guo, J.; Chang, S.; Wang, X.; Zhou, J.; Liang, F.; he, J. *Phys. Chem. Phys.* **2019**, *21*, 15940-15948.
- (41). Yang, W. R.; Gooding, J. J.; Hibbert, D. B. J. Electroanal. Chem. **2001**, *516*, 10-16.
- (42). Kim, J.; Kim, B. K.; Cho, S. K.; Bard, A. J. J. Am. Chem. Soc. 2014, 136, 8173-8176.
- (43). Mukherjee, R.; Huang, Z.-F.; Nadgorny, B. Appl. Phys. Lett. **2014**, 105, 173104.
- (44). Chen, C.; Ravenhill, E. R.; Momotenko, D.; Kim, Y.; Lai, S.; Unwin, P. R. *Langmuir* **2015**, *31*, 11932-11942.
- (45). Zhou, Y. G.; Rees, N. V.; Compton, R. G. Angew. Chem., Int. Ed. **2011**, *50*, 4219-4221.
- (46). Kleijn, S. E.; Lai, S.; Koper, M.; Unwin, P. R. Angew. Chem., Int. Ed. 2014, 53, 3558-3586.
- (47). Duan, G.; Zhang, Y.; Luan, B.; Weber, J. K.; Zhou, R. W.; Yang, Z.; Zhao, L.; Xu, J.; Luo, J.; Zhou, R. Sci. Rep. 2017, 7, 42767.
- (48). Mingzhi; Li; Zhiqiang; Ge; Shudong; Zhang; Peng; He; Yaxiong; Gu *Chemelectrochem* **2018**, *5*, 3021-3027.
- (49). van Schrojenstein Lantman, E. M.; Deckert-Gaudig, T.; Mank, A. J.; Deckert, V.; Weckhuysen, B. M. *Nat. Nanotechnol.* **2012,** *7*, 583.
- (50). Lim, C. Y.; Owens, N. A.; Wampler, R. D.; Ying, Y.; Granger, J. H.; Porter, M. D.; Takahashi, M.; Shimazu, K. *Langmuir* **2014**, *30*, 12868-12878.
- (51). Ren, B.; Picardi, G.; Pettinger, B. Rev. Sci. Instrum. 2004, 75, 837-841.
- (52). Pettinger, B.; Domke, K. F.; Zhang, D.; Schuster, R.; Ertl, G. *Phys. Rev. B* **2007**, *76*, 113409.
- (53). Wang, X.; Huang, S.-C.; Huang, T.-X.; Su, H.-S.; Zhong, J.-H.; Zeng, Z.-C.; Li, M.-H.; Ren, B. *Chem. Soc. Rev.* **2017**, *46*, 4020-4041.
- (54). Lin, K.-Q.; Yi, J.; Zhong, J.-H.; Hu, S.; Liu, B.-J.; Liu, J.-Y.; Zong, C.; Lei,
- Z.-C.; Wang, X.; Aizpurua, J.; Esteban, R.; Ren, B. Nat. Commun. 2017, 8, 14891.
- (55). Domke, K. F.; Zhang, D.; Pettinger, B. J. Phys. Chem. C 2007, 111, 8611-8616.

- (56). Liu, Z.; Ding, S.-Y.; Chen, Z.-B.; Wang, X.; Tian, J.-H.; Anema, J. R.; Zhou,
- X.-S.; Wu, D.-Y.; Mao, B.-W.; Xu, X. Nat. Commun. 2011, 2, 1-6.
- (57). Hao, J.; Han, M.-J.; Li, J.; Meng, X. J. Colloid Interface Sci. 2012, 377, 51-57.
- (58). Cline, G. W.; Hanna, S. B. J. Org. Chem 1988, 53, 3583-3586.
- (59). Satterthwait, A. C.; Jencks, W. P. J. Am. Chem. Soc. 1974, 96, 7018-7031.
- (60). Cline, G. W.; Hanna, S. B. J. Am. Chem. Soc. 1987, 109, 3087-3091.
- (61). Kurouski, D.; Postiglione, T.; Deckert-Gaudig, T.; Deckert, V.; Lednev, I. K. *Analyst* **2013**, *138*, 1665-1673.
- (62). Nakajima, N.; Ikada, Y. Bioconjug. Chem. 1995, 6, 123-130.
- (63). de Oteyza, D. G.; Gorman, P.; Chen, Y.-C.; Wickenburg, S.; Riss, A.; Mowbray, D. J.; Etkin, G.; Pedramrazi, Z.; Tsai, H.-Z.; Rubio, A. *Science* **2013**, 1238187.
- (64). Skoog, D. A.; Holler, F. J.; Crouch, S. R., *Principles of instrumental analysis*. Cengage learning: 2017.
- (65). Tuchband, M.; He, J.; Huang, S.; Lindsay, S. Rev. Sci. Instrum. 2012, 83, 015102.
- (66). Rodríguez-Lorenzo, L.; Alvarez-Puebla, R. A.; Pastoriza-Santos, I.; Mazzucco, S.; Stéphan, O.; Kociak, M.; Liz-Marzán, L. M.; García de Abajo, F. J. *J. Am. Chem. Soc.* **2009**, *131*, 4616-4618.
- (67). Chang, S.; Huang, S.; He, J.; Liang, F.; Zhang, P.; Li, S.; Chen, X.; Sankey, O.; Lindsay, S. *Nano Lett.* **2010**, *10*, 1070-1075.
- (68). Plesa, C.; Dekker, C. Nanotechnology 2015, 26, 084003.

TOC Graphic

